Bull Volcanol (2015) 77:52
DOI 10.1007/s00445-015-0934-y

RESEARCH ARTICLE

Emplacement of the Cabezo María lamproite volcano (Miocene, SE Spain)

Thomas M. Gernon[1] · Samuel Spence[1] · Clive N. Trueman[1] · Rex N. Taylor[1] · Eelco Rohling[1,2] · Stuart J. Hatter[1] · Ian C. Harding[1]

Received: 8 December 2014 / Accepted: 27 April 2015

Abstract Lamproite volcanoes are uncommon in the geological record but are exceptionally well preserved in the Betic Cordilleras of SE Spain, where they erupted during the Late Miocene (Tortonian to Messinian stages). The parent melts are thought to have been channelled through major lithospheric faults to erupt at or near the faulted margins of Neogene sedimentary basins. Lamproite magmas are thought to be relatively CO_2-poor (<1 wt%) and are typically characterised by an effusive eruption style and the development of lava lakes and scoria cones. Cabezo María is a relatively small (∼550 m diameter) lamproite volcano that was emplaced within the shallow-water marine-influenced Vera Basin. The lamproites are compositionally similar to those of the Roman Province and generally less potassic (K_2O<5 wt%) than other (ultra-) potassic rocks in SE Spain (e.g. Cancarix, Fortuna). The initial eruption stages were dominated by explosive magma-water interactions and the formation of peperites. These are characterised by angular fragments of glassy lamproite lavas (and isolated lobes) incorporated in sediments, locally showing the effects of thermal metamorphism. Further, elutriation pipes and 'jigsaw-fit' textures are observed in the peperites. The lavas and peperites are overlain by outward-dipping well-stratified scoria deposits defining part of a cinder cone, which is inferred to have emerged above sea level. Steep internal contacts with inward-dipping, structureless breccias likely represent the inner wall deposits of a central conduit. The deposits are cross-cut by late-stage dykes, which supplied fissure eruptions of geochemically similar lavas capping the scoria cone. The transition from explosive to effusive behaviour may reflect the decreased availability of water, possibly due to downward migration of the feeder conduit below the level of water-saturated sediments.

Keywords Lamproite · Volcano · Eruption · Peperite · Scoria cone

Introduction

Lamproite rocks have attracted significant economic interest as hosts to diamonds and given their deep origins (≥150 km) offer important insights into mantle evolution and lithospheric-scale processes. Cabezo María (37°12′ 43.3″N, 1°55′56.9″W; 225-m elevation) is an eroded lamproite volcano that outcrops in the Vera Basin in southeastern Spain. The occurrence, first described by Fúster and De Pedro (1953) and not well understood in terms of volcanological emplacement, is part of a cluster of approximately ten volcanic edifices of potassic and ultrapotassic composition in the Betic Cordilleras (Fig. 1). Collectively, these are thought to have been active over a period of almost 2 Ma (8.3–6.7 Ma; Montenat et al. 1975; Turner et al. 1999), and locally exhibit a marked cluster in activity around 7.3–7.2 Ma (Playà and Gimeno 2006). Seghedi et al. (2007) suggest that lamproite emplacement was tectonically controlled as they occur principally along the margins of extensional intramontane basins, which

Editorial responsibility: S. Calvari

✉ Thomas M. Gernon
Thomas.Gernon@noc.soton.ac.uk

[1] Ocean and Earth Science, University of Southampton, Southampton, SO14 3ZH, UK

[2] Research School of Earth Sciences, The Australian National University, Canberra, ACT. 2601, Australia

Published online: 28 May 2015

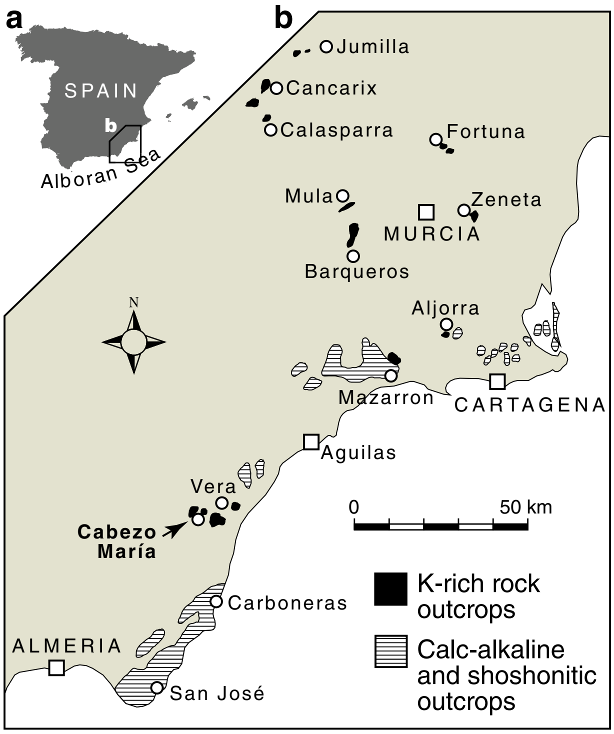

Fig. 1 **a** Inset map of Spain showing location of **b** the Betic Cordilleras illustrating potassic and calc-alkaline/shoshonitic outcrops, including Cabezo María

served as depocentres for Neogene sedimentation. Lamproite magma ascent is thought to have been accommodated by lithospheric-scale faulting accommodating subduction rollback (Pérez-Valera et al. 2013).

Cabezo María erupted during the Tortonian to Messinian stages of the Miocene epoch. Lava flows in the lower part of the sequence are interbedded with Messinian marls and turbidites (i.e. $\lesssim$7.246 Ma)—an observation that is difficult to reconcile with early K-Ar dates of 8.6 Ma (Nobel et al. 1981). More recently, a radiometric age of 7.45 $\pm$ 0.08 Ma has been reported (Bellido Mulas and Brändle Matesanz 2011). This discrepancy of $\sim$1 Ma might suggest that the volcano was active over an extended period, similar to other lamproite centres in the region, for example, Barqueros (Fúster and Gastesi 1965) and Cerro del Monagrillo at Las Minas de Hellín (Gimeno 1994). Further, at Cabezos Negros, two successive eruptions of lamproite magmas were separated by a hiatus of approximately 1 Ma (see Playà and Gimeno 2006 and references therein).

Here, lamproites are defined as potassic and ultrapotassic (i.e. $K_2O/Na_2O>3$) volcanic rocks, typically sourced from the mantle (>150 km) and closely linked (genetically, compositionally and texturally) to kimberlites and lamprophyres. Relative to intraplate basaltic magmas, lamproites are characterised by high Mg and low Al, Fe and Ca and a marked enrichment in incompatible elements (Mitchell and Bergman 1991). The lamproites of SE Spain were emplaced at the end of a major extensional event following emplacement of the Alboran Domain to the south onto the Iberian platform (Turner et al. 1999). The parent magmas experienced a complex, multi-stage history (Venturelli et al. 1984; Turner et al. 1999), involving melt extraction from a source region at <2.5 GPa, and successive metasomatic enrichment events (Mitchell and Bergman 1991; Turner and Hawkesworth 1995).

Lamproite magmas are commonly regarded as CO_2-poor (Dawson 1987), probably on the order of <1 wt%. The key volatile species are H_2O and F, when combined have a solubility of 3–10 wt% even at near-surface pressures (>0.5 km; Mitchell and Bergman 1991). Lamproites are typically associated with effusive eruptions and the development of lava lakes, lava fields and monogenetic scoria cones (Mitchell and Bergman 1991). Although these physical characteristics set lamproites apart from their kimberlite counterparts, it is now clear that the latter may deviate from typical explosive (i.e. diatreme-forming) behaviour (e.g. Igwisi Hills, Tanzania; Brown et al. 2012), exhibiting many features more commonly associated with monogenetic basaltic volcanism (e.g. Hintz and Valentine 2012). Therefore, there are likely more overlaps in eruptive style between some lamproites, kimberlites and basalts than has previously been appreciated (see Brown and Valentine 2013). This paper describes the deposits of the well-preserved Cabezo María volcano (Fig. 2), where field relationships suggest that the lamproites initially erupted hydrovolcanically within a shallow-water marine-influenced basin.

Methods

Fieldwork and sampling of Cabezo María was undertaken in March 2011, 2012 and 2015. The structure and composition of volcanic outcrops were mapped at a scale of 1:2000 using aerial photographs. Representative samples were taken for the purposes of petrographic (optical transmitted light microscopy) and geochemical analysis. Whole-rock major and trace elements were analysed using X-ray fluorescence (XRF) (Panalytical Magix-Pro WD-XRF fitted with a 4-kW Rh X-ray tube) at the University of Southampton. Solution inductively coupled plasma mass spectrometry (ICP-MS) was carried out to determine the concentration of incompatible elements using a ThermoScientific XSeries2 at the University of Southampton. The samples were prepared in accordance to the standard procedure of silicate rock dissolution by HF digest, adapted from Beauchemin (2008). In this paper, we adopt the terms used to describe lamproites from Mitchell and Bergman (1991), and in describing peperites, we follow terminology introduced by Skilling et al. (2002).

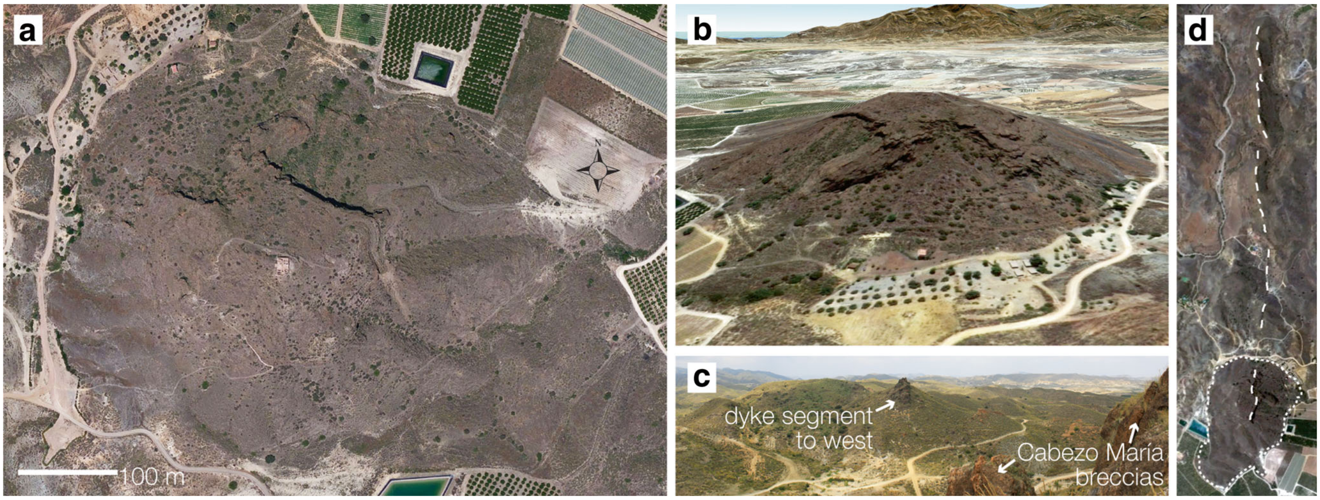

Fig. 2 **a** Aerial photograph of the Cabezo María volcano and **b** oblique aerial image looking SSE (from GoogleEarth Pro); note the presence of lava flows capping the volcanic construct and in places preserving the underlying scoria cone deposits; **c** panoramic photograph looking west (taken from breccias on the southern flanks of Cabezo María) showing a dyke segment to the west, which appears to be an *en echelon* continuation of the dyke exposed at the summit of Cabezo María (**d**)

Petrography and geochemistry

The rocks investigated in this study are all classified as lamproites based on their major element concentrations (notably low CaO; see Table 1) and have previously been termed 'verites' (Fúster and De Pedro 1953). The lamproites contain olivine (>Fo_{90-95}) and phlogopite phenocrysts in a glassy groundmass (typically >70 vol.%) with very small phlogopite crystals. Other phases present in the groundmass include diopside, sanidine and leucite. Vesicles are infilled with secondary calcite. Some larger xenocrystic olivine contains spinel inclusions (of suspected upper mantle origin). The groundmass contains glass, phlogopite, sanidine, clinopyroxene and apatite.

The rocks exhibit moderate K_2O and high Na_2O contents compared to other occurrences in SE Spain and mainly plot within the potash series (after Middlemost 1975), overlapping with lamproites of Vera and Jumilla (Fig. 3a). Other potassic and ultrapotassic rocks in the region (e.g. Cancarrix, Fortuna, Barqueros and Mazarron; see Duggen et al. 2005) generally exhibit higher K_2O contents (>5 wt%). The Cabezo María rocks are metaluminous and relatively rich in SiO_2 (>42 wt%), plotting in the same field as lamproites of the Roman Province (Fig. 3b, Barton 1979), which similarly contain pyroxene and sanidine.

The REE trace-element patterns of the lamproites are distinctive (Fig. 4), showing a similar pattern to other lamproites of the Vera cluster (Turner et al. 1999) and are significantly higher than the Neogene calc-alkaline volcanics, for example, Cabo de Gata to the south (Fig. 1b). In particular, they exhibit extreme enrichment in incompatible trace elements, which has been attributed to a multi-stage history of the mantle source involving successive extraction and enrichment events (see Turner et al. 1999). This complex history appears to be consistent with that of the Ronda (Spain) and Beni Bousera (Morocco) peridotites (Pearson et al. 1991).

Field observations

The Cabezo María volcano (Figs. 2a, b and 5) has a present maximum diameter of ~550 m, a mimumum surface area of 1.6×10^5 m^2 and an estimated minimum volume of 3.5×10^6 m^3. Although it has experienced (limited) erosion, the low-key topographic expression makes the construct similar in appearance and scale to small monogenetic scoria cones (e.g. Hintz and Valentine 2012). Further, the volcano appears to be localised along a segmented dyke system (Fig. 2c, d), similar to, for example, basaltic conduits in the San Rafael Swell, Utah (Kiyosugi et al. 2012). The Cabezo María volcanics are hosted by Messinian marls deposited in an intermontane basin (Vera Basin), which remained connected to the Mediterranean Sea through Miocene times with the exception of the Messinian salinity crisis (see Alonso-Zarza et al. 2002 and references therein). As such the lamproites were emplaced into a shallow-water environment subject to marl deposition and minor clastic input.

At Cabezo María, peperites—products of magma-sediment mixing—are dominantly lower in the sequence (from 140 to 170 masl), although some minor outcrops occur higher up the flanks (~200 masl). The peperites are overlain by massive, blocky lavas, some of which are columnar jointed. These are overlain by well-bedded scoria deposits, which in turn are capped by late-stage lavas. The

Table 1 Major and trace element data for Cabezo María volcanics

Wt%	CM1 Blocky lava	CM3 Massive lava	CM4 Vesicular dyke	CM5a Lava breccia	CM5b Massive lava	CM5c Massive lava	CM2 Peperite (sediment-veined)	JA-2 Measured	JA-2 Recom. value	BRR-1 Measured	BRR-2 (Murton et al. 2002)
SiO_2	58.95	59.30	57.36	57.75	58.85	55.81	33.73			49.62	49.82
TiO_2	1.45	1.47	1.40	1.47	1.45	1.40	0.84			1.02	1.03
Al_2O_3	11.96	12.05	11.54	11.80	11.66	11.37	6.66			14.21	14.37
Fe_2O_3	4.74	3.95	4.86	4.91	5.33	5.99	3.80			11.84	11.88
MnO	0.07	0.05	0.07	0.08	0.07	0.09	0.13			0.20	0.18
MgO	3.94	2.53	4.72	3.07	5.41	3.48	1.77			8.59	8.57
CaO	3.51	4.19	4.76	4.65	2.74	4.29	25.48			12.06	11.95
Na_2O	3.09	2.74	3.16	3.31	2.94	2.34	1.04			1.99	1.97
K_2O	4.09	4.50	3.61	3.58	4.53	5.12	1.45			0.05	0.05
P_2O_2	0.82	0.81	0.78	0.84	0.82	0.79	0.46			0.08	0.09
SO_2	0.09	0.14	0.01	0.02	0.00	0.03	0.10			0.18	
LOI	6.42	7.15	7.03	7.66	7.50	7.52	23.97				
Total	99.13	98.87	99.29	99.13	101.31	98.25	99.42			99.84	99.93
ppm											
Li	22.2	16.0	22.6	23.3	20.9	28.0	3.8	29.7	27.3	5.2	5.4
Sc	14.7	13.8	14.6	15.4	13.7	14.7	20.2	18.5	19.6	45.38	45.87
V	87.3	85.9	86.4	89.1	85.1	87.7	47.3	112	126	312	323
Cr	505	528	592	577	646	534	274	389	436	384	384
Co	25.3	17.7	27.4	28.3	26.2	24.0	12.8	28	30	50	48
Ni	357	250	362	365	291	289	155	127.5	135	130	133
Cu	19.8	17.7	30.6	24.4	20.9	27.1	13.7	31.0	28.1	89.8	86.1
Zn	66.9	62.2	64.4	67.3	70.2	67.8	73.0	61.9	65.0	87.0	85.2
Rb	607	592	570	631	579	586	207	78.7	72.9	0.6	0.6
Sr	448	501	445	435	458	463	684	251.4	248.0	67.3	71.2
Y	24.3	24.3	23.6	24.7	23.4	24.6	19.3	17.8	18.3	28.3	27.4
Zr	782	797	751	799	769	814	414	118.9	116.0	55.2	54.9
Nb	41.5	43.4	40.1	43.2	41.5	43.6	21.8	9.22	9.47	1.09	1.19
Cs	128	159	104	98	96	313	104	5.2	4.6	0.007	0.005
Ba	1674	1815	1552	1676	1641	1644	748	325	321	6.89	6.55
La	102	107	102	103	105	108	60	16.22	15.80	1.58	1.62
Ce	289	298	278	297	287	298	167	33.91	32.70	5.20	5.39
Pr	39.7	40.7	38.3	40.5	39.4	40.7	22.8	3.86	3.84	0.99	1.01
Nd	166	170	160	170	165	170	97	14.63	13.90	5.75	5.68
Sm	29.2	29.8	28.0	29.8	29.0	29.6	17.7	3.15	3.11	2.30	2.17
Eu	4.5	4.6	4.3	4.6	4.5	4.6	2.9	0.91	0.93	0.87	0.81
Gd	13.9	14.2	13.5	14.2	13.7	14.3	9.0	3.09	3.06	3.45	3.25
Tb	1.38	1.39	1.33	1.41	1.36	1.41	0.95	0.48	0.44	0.64	0.63
Dy	5.68	5.73	5.47	5.77	5.51	5.70	4.14	2.91	2.80	4.40	4.26
Ho	0.87	0.88	0.85	0.88	0.85	0.88	0.68	0.61	0.50	0.99	0.98
Er	2.08	2.09	2.03	2.05	1.99	2.08	1.70	1.71	1.48	2.90	2.86
Tm	0.28	0.28	0.28	0.28	0.27	0.28	0.24	0.26	0.28	0.45	0.43
Yb	1.72	1.70	1.69	1.73	1.63	1.70	1.52	1.70	1.62	2.93	2.79
Lu	0.24	0.24	0.24	0.24	0.23	0.25	0.22	0.26	0.27	0.45	0.44
Hf	20.1	20.6	19.4	20.6	20.0	20.7	10.4	2.94	2.86	1.56	1.55

Table 1 (continued)

Wt %	CM1 Blocky lava	CM3 Massive lava	CM4 Vesicular dyke	CM5a Lava breccia	CM5b Massive lava	CM5c Massive lava	CM2 Peperite (sediment-veined)	JA-2 Measured	JA-2 Recom. value	BRR-1 Measured	BRR-2 (Murton et al. 2002)
Ta	3.2	3.5	3.2	4.6	3.4	4.8	1.7	0.79	0.80	0.16	0.06
Pb	79.3	108.7	66.1	93.3	164.7	230.4	54.1	22.21	19.20	0.35	0.38
Th	98.7	101.7	94.5	99.7	96.8	99.1	45.9	4.88	5.03	0.064	0.051
U	21.0	21.7	20.2	21.0	21.1	21.8	13.4	2.25	2.21	0.045	0.038

Major elements measured by XRF and trace elements by ICP-MS at the University of Southampton. Analyses of International Standard JA-2 (Imai et al. 1995) and Southampton internal basalt standard BRR-1 (Murton et al. 2002) are presented with consensus values for these rocks to assess accuracy. Sample CM2 contains millimetre to centimetre-scale veins of carbonate sediment entrained during emplacement, and the data is presented for comparison

latter (Fig. 2b) appear to overlie steep lava breccia bodies, thought to represent the inner wall deposits of the central conduit. The deposits are intruded by steep-dipping vesicular dykes, which likely erupted as fissures producing lava flows in the highest part of the sequence.

Basal peperites

Peperites generally occur lower in the sequence where lamproite fragments are intimately mixed with marls and micaceous sandstones (Fig. 6), which locally comprise lithified plant fragments (some 2 cm in diameter). In terms of two-dimensional morphology, the peperites range from irregular to pod-like (sensu Skilling et al. 2002). Most commonly, highly angular and sub-angular fragments of (glassy) lava are fully enclosed by sediments (Figs. 6 and 7a) resulting in a 'dispersed' internal structure (Skilling et al. 2002). The fragments range in size from 0.5 to 40 cm, with vesicles (∼ 10 %) concentrated around the margins. In places, coherent domains (i.e. unbrecciated lava) are penetrated by elutriation pipes (Fig. 7b); these are generally thin structures (i.e. 2–10 cm) and consist of very fine to fine-grained sediment, and angular juvenile clasts sharing the same composition as the coherent host-rock. The coherent domains underlie the peperites and locally appear to have caused updoming of sediments into which they presumably intruded and mingled together within a boundary zone (Fig. 6).

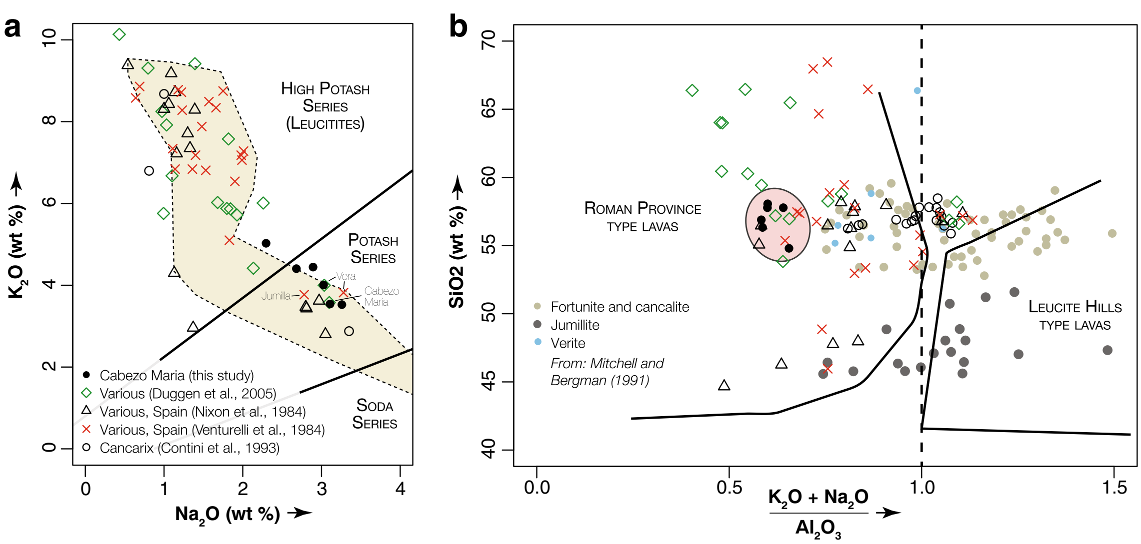

Fig. 3 **a** K_2O versus Na_2O diagram (after Middlemost 1975) plotting lamproites from Cabezo María and showing their relationship to other (ultra-) potassic rocks in SE Spain (Venturelli et al. 1984; Nixon et al. 1984; Contini et al. 1993; Duggen et al. 2005); note that the coloured field shows the Murcia–Almería lamproite trend (Fúster and Gastesi 1965; Venturelli et al. 1984) as shown in Mitchell and Bergman (1991). **b** SiO_2 versus the peralkalinity index for lamproites of Cabezo María, classified as Roman Province type (sensu Barton 1979), compared to other lamproitic and related rocks (e.g. verite, fortunite and jumillite) of SE Spain (see **a** for key to symbols)

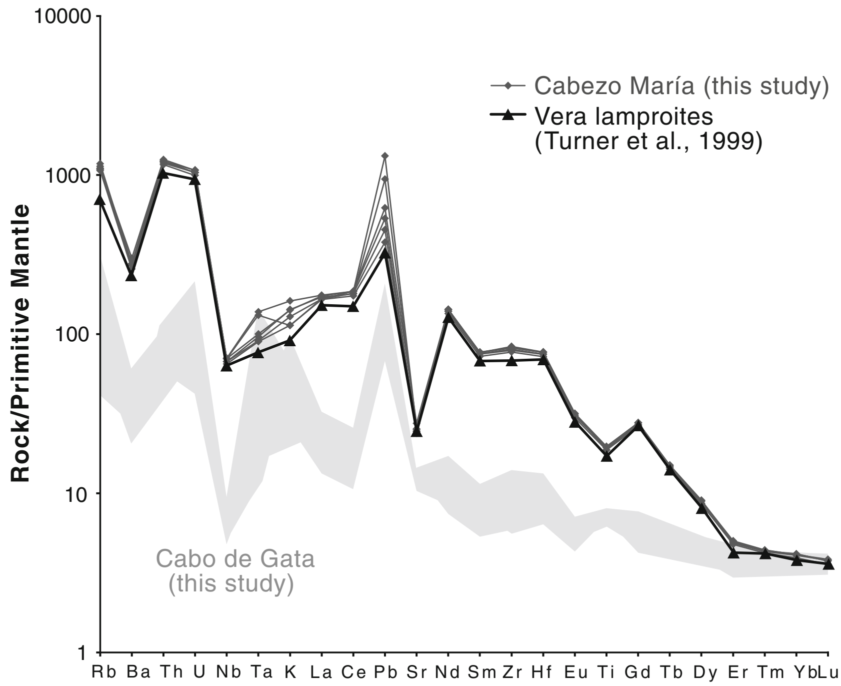

Fig. 4 Plots of REE and trace-element distribution patterns of the Cabezo María lamproites, normalised to average primitive values from Hofmann (1988) and Sun (1982). Data from the Vera lamproite is from Turner et al. (1999); the field of calc-alkaline volcanics of Cabo de Gata (this study) is shown for comparison purposes only

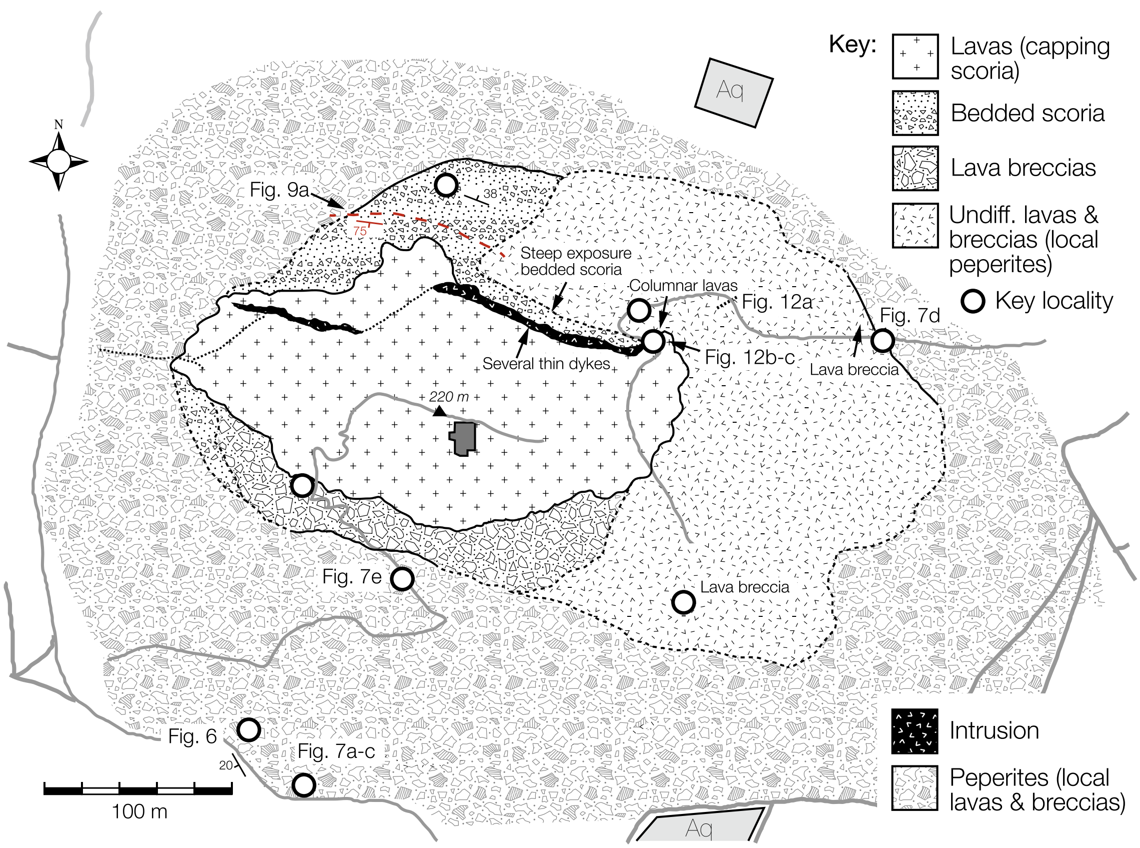

Fig. 5 Simplified geological map of the Cabezo María lamproite volcano showing the distribution of key units (*Aq* water reservoir). Note that the area and volume estimates provided in the accompanying text do not include extrusive lithofaces (e.g. peperites), the true aerial extent of which are unknown (note extensive citrus groves)

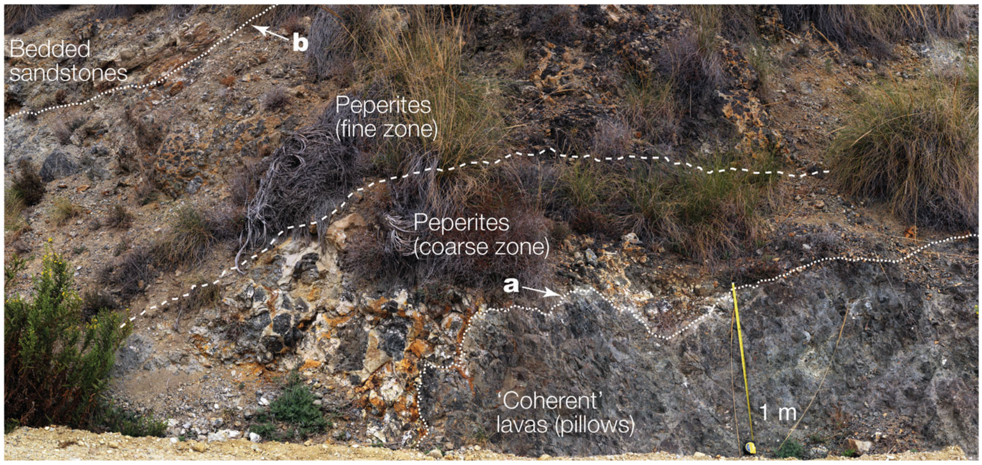

Fig. 6 Field photographs of an exposure showing **a** the irregular contact between 'coherent' lavas and peperites. Note the presence of a 'coarse zone' immediately adjacent to coherent lavas and an overlying 'fine zone' in contact **b** with bedded sandstones; it appears that sedimentary beds have locally been uplifted by the underlying peperites

In places, the lavas take the form of discrete pillow-like lobes up to one metre in diameter (Fig. 7c, note concentrically aligned vesicles) in many cases isolated and completely enclosed in sediment (Fig. 7d). Less typically (higher up slope at ∼200 masl, Fig. 5), the morphology could be described as jigsaw-fit (Fig. 7e), with sediments injected into thin cracks (1–5 cm thick) in the lavas. The sediments in the interstices between clasts, typically yellow-orange in colour, appear to be baked in places with a conchoidal fracture pattern and strong discolouration adjacent to lava fragments (Fig. 8a). Some thin regions (typically >1 mm wide) surrounding juvenile fragments have experienced recrystallisation (Fig. 8b) and these zones exhibit possible vesiculation (vesicle diameters <500 μm). Original sediment textures and structures were not observed in the peperite domains.

Bedded scoria deposits

To the NE of the Cabezo María edifice (Figs. 2b and 5), a steep-sided rock face (∼10–15 m high; Fig. 9a)

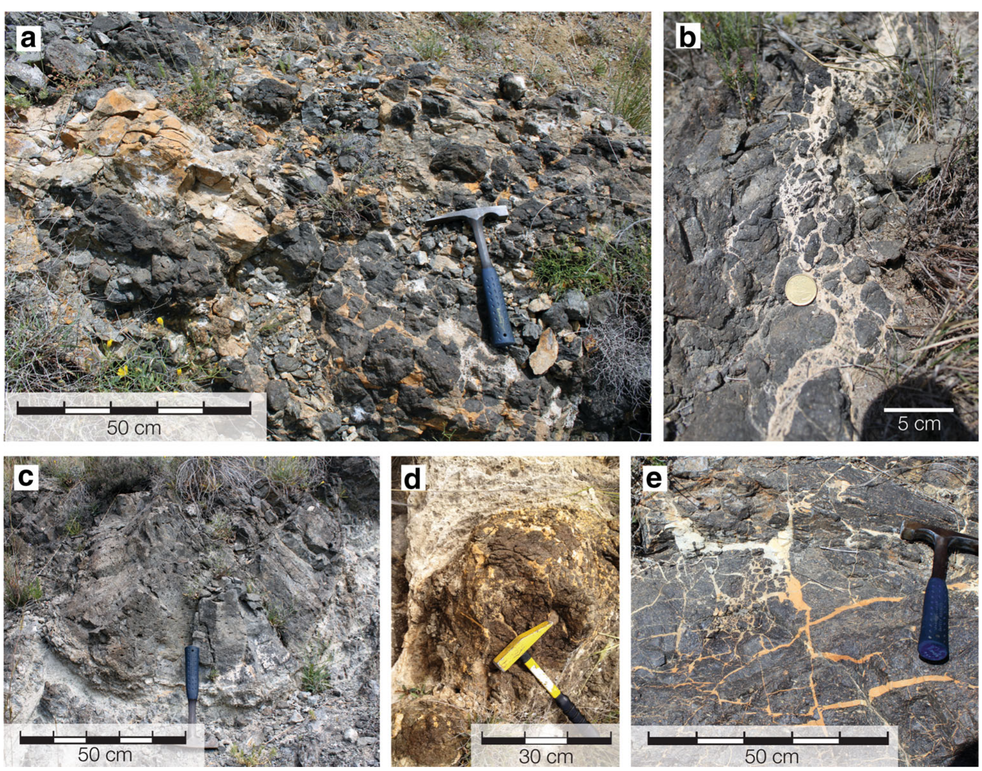

Fig. 7 Field photographs of peperites from Cabezo María. **a** Fragments of dispersed lamproite encapsulated by sediments. **b** Elutriation pipe invading 'coherent' lamproite lavas in the vicinity of peperite exposure shown in (**a**). **c** Well-defined pillow lava in a coherent domain; note concentrically aligned vesicles. **d** Isolated pillow lobe encapsulated by sediment. **e** Jigsaw-fit lava with sediments in-filling cracks

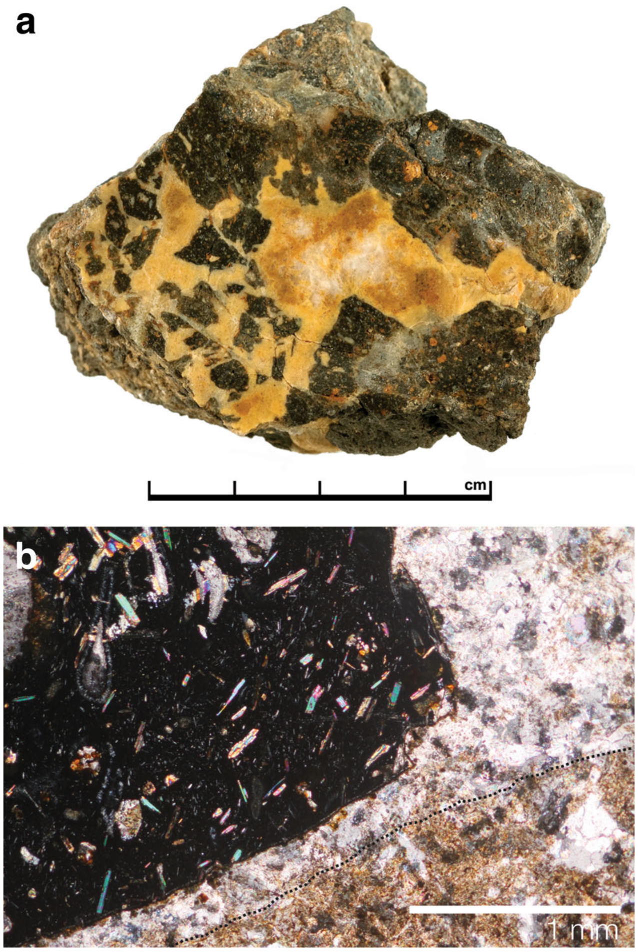

Fig. 8 **a** Photograph a hand specimen of peperite (sample CM2) from the locality shown in Fig. 7a. Note the angularity and glassy nature of clasts and sharp contacts with host sediments. **b** Photomicrograph of a lamproite clast from (**a**) showing a thin chilled glassy rim to the juvenile clast, which internally exhibits a trachytic texture, and recrystallisation of sediments adjacent to the clast

exposes a succession of well-stratified tuffs and lapilli tuffs comprising (agglutinated) scoria and occasional spatter bombs. The deposits dip at a high angle (33°–38°) towards the north away from the centre of the edifice, defining a scoria cone-like geometry, and are capped by lava flows. The dipping sequence is offset in places by minor normal faults (Fig. 9a), and other steep internal contacts nearer the centre of the edifice, which juxtapose contrasted packages of tuffs and breccias (Fig. 9b).

The scoria deposits (Fig. 10) are moderately to poorly sorted, comprising angular lamproite clasts (Fig. 11a). The beds are distinctive from the underlying peperites, as they lack juvenile clasts with well-developed chilled margins, in addition to pillow-lobes and interstitial sediments. The bedding is typically 30–50 cm thick (Figs. 9a and 10) and is crudely developed appearing more structureless in places. In most cases, bedding is defined by variations in clast size and organisation (Fig. 10), together with the occurrence of large (~50 cm diameter) degassed slabs of lava restricted to certain beds (Fig. 11a).

Massive breccia deposits

The southern path to the hermitage traverses through breccia bodies near the summit of Cabezo María (Fig. 5). The breccias comprise angular clasts (see Fig. 11b), typically <10 cm in diameter and generally ranging from 2 to 5 cm. The breccias are monolithologic consisting of vesicular juvenile lamproite clasts, many glassy in appearance. In general, the breccias are clast supported (Fig. 11b), although locally there are matrix-supported patches, with the matrix consisting of very fine- to fine-grained altered ash. The breccias are most commonly structureless, and the component clasts do not exhibit any strong preferred orientations. However, it is possible to discern several subtle internal contacts in the breccia bodies, typically marking variations in clast proportions or sizes. Unfortunately, due to limited exposure, it is not possible to follow these contacts over any great distance.

Uppermost lavas and intrusions

Lavas and dykes (Fig. 12) exposed at the summit of Cabezo María are petrologically very similar, consisting of (carbonated) olivine, phlogopite, pyroxene and some vesicles with secondary calcite infill (Fig. 12e). In general, the phlogopites are platy and exhibit flow alignment textures (see Fig. 8b). The lavas are similar to many basaltic lavas, in that they exhibit scoriaceous flow-tops with ropey flow structures, small lava tubes defined by a thin solidified 'crust' of lava immediately underlain by a cavity (Fig. 12b) and columnar jointing (Fig. 12c). The columns are developed perpendicular to the irregular basal surface, dipping approximately 70° towards 330 NW (~100 m NE of hermitage, see Fig. 5). At the base of the flow, vesicles are aligned roughly parallel to the basal contact (i.e. perpendicular to columns). The lavas are generally massive but locally brecciated, most likely due to columnar jointing and flow-induced brecciation.

The dykes are typically 0.5–1 m wide (Fig. 12a) and thicken to ~2–3 m in the west (see Fig. 2c). The dykes are moderately crystal rich (~20 %) and contain autoliths of more crystal-rich lamproite (~30–40 %), presumably representing pre-existing lavas from lower down in the stratigraphy (Fig. 12d). The dykes are moderately vesicular, with stretched and elongated vesicles ranging in diameter from 1 to 20 mm, and oriented parallel to the intrusion contacts (Fig. 12d).

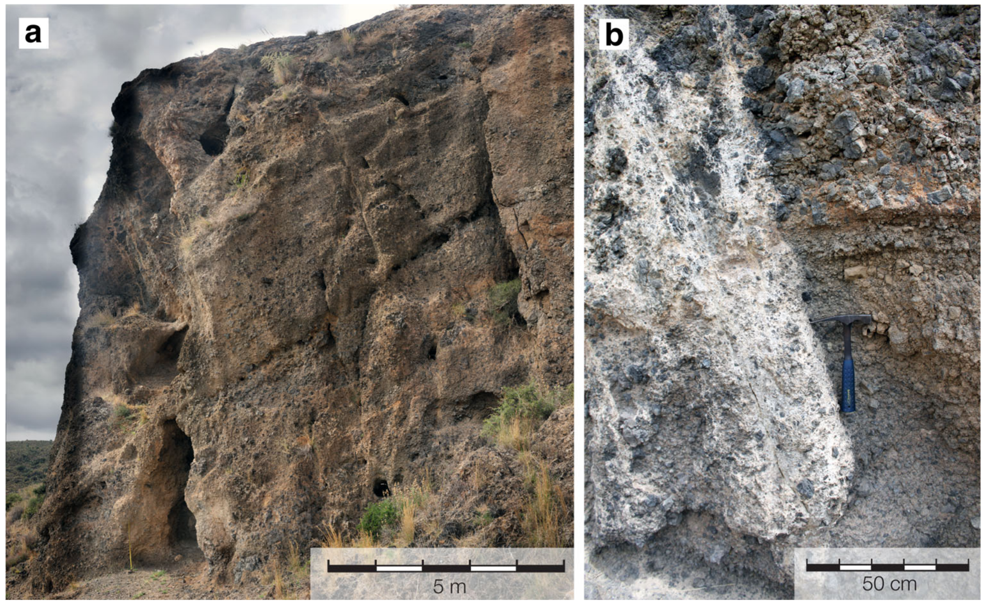

Fig. 9 **a** Field photograph of bedded scoria deposits exposed in a rock face to the north of Cabezo María (see Fig. 2b); note the presence of well-stratified tuffs and breccias, and minor normal faults. **b** Steep and sharply defined internal contact between altered tuffs (*left*) and layered breccias (*right*)

Discussion

We propose that the Cabezo María lamproite volcano was emplaced in at least three key stages, involving initial explosive hydromagmatic eruptions, an emergent phase involving cone-forming Strombolian eruptions and a final phase of effusive lava flow emission (see Fig. 13).

Stage 1: hydromagmatic eruptions

Deposits low in the sequence exhibit a number of features consistent with emplacement as peperites. The dispersed structure (e.g. Fig. 7a) and apparent destruction of sedimentary structures in local regions adjacent to clasts can be explained by sediment fluidisation associated with magma emplacement into the sediment pile. In most cases, discrete clasts exhibit quenched glassy margins and contact metamorphism of sediments adjacent to clasts (Fig. 8). The well-developed elutriation pipes (Fig. 7b) provide further evidence of intense sediment fluidization by superheated steam and volatiles (cf. Kokelaar 1982). Elsewhere in the Vera Basin, there is evidence that lavas of similar age and composition flowed out over unconsolidated water-saturated sediments (Völk 1967).

Based on the observed field relationships, eruptions at Cabezo María were initially sub-aqueous, recording the development of a fissure complex and its interaction with unconsolidated basinal sediments. This behaviour is analogous to diamondiferous lamproite diatremes in Argyle (NW Australia), where magmas interacted explosively with incohesive water-saturated sediments (Boxer et al. 1986; Stachel et al. 1991). Similarly, magma-water interactions occur exclusively during the earliest eruptive stages at analogous basaltic scoria cones (e.g. Rothenberg, East Eifel; Houghton and Schmincke 1989). It is likely that the feeder intrusion(s) rapidly developed into a steep-sided vent (Lorenz 2003) due to persistent explosive flows, erosion and wall instability (Sparks et al. 2006). The abundance of blocky quenched clasts dispersed in host sediments can be explained by fragmentation resulting from explosive magma-water interactions (Busby-Spera and White 1987). Field relationships (Fig. 6) suggest that the magmas were intruded along sediment bedding planes, locally mixing with sediments (in a boundary zone) and forming pillow lavas in more coherent domains (cf. Iberian Copper Belt; Boulter 1993; Boulter et al. 1999). Elsewhere, isolated lava 'lobes' fully surrounded by sediment (Fig. 7d) are more readily explained by shedding of subaqueously erupted lavas into unconsolidated sediments, likely within a very shallow-water environment. The jigsaw-fit textures higher in the sequence are consistent with in situ quench fragmentation of lavas, most likely due to seawater incursion (see Skilling et al. 2002 and references therein).

Stage 2: volcano emergence and growth

The bedded scoria deposits overlying the basal peperites and lavas are interpreted to represent the outer wall of a dissected scoria cone. Here, the absence of quench glass, jigsaw-fit fractures, chilled margins to juvenile clasts, sediment interactions and pillow-lobes (all observed in the basal peperite sequence) all suggest a transition to subaerial deposition. Accordingly, each bed (Fig. 11a) likely represents a discrete eruptive event, presumably of Strombolian intensity (e.g. Houghton and Schmincke 1989). Although the central vent is not particularly well exposed, steep internal contacts

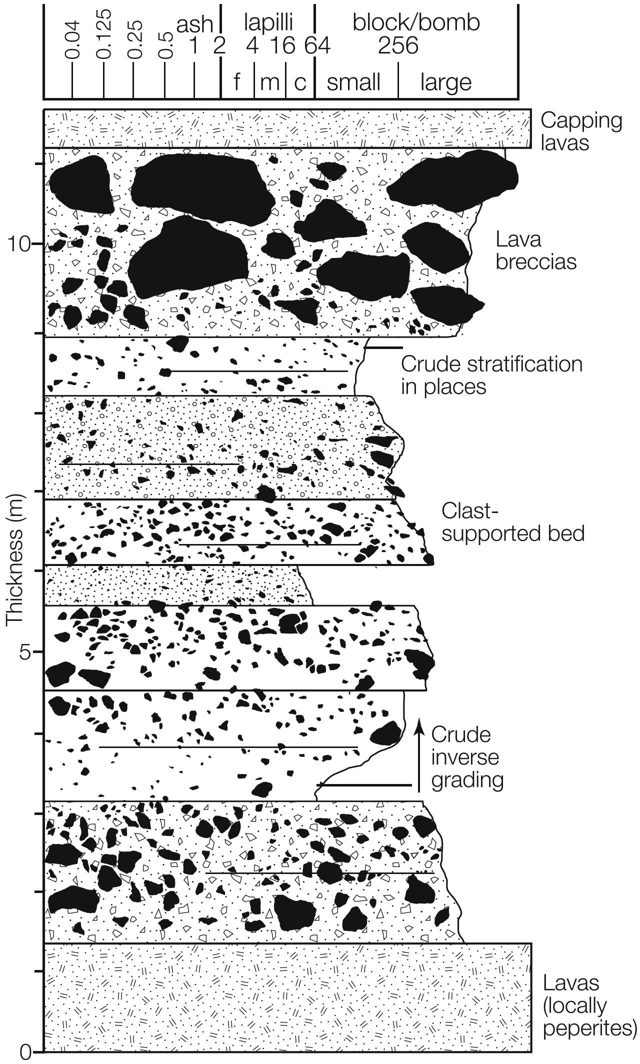

Fig. 10 Schematic graphic log showing the bedding and clast distribution within the scoria cone sequence shown in Fig. 9a

are observed between bedded scoria and breccia bodies (e.g. Fig. 9b), which are similar to structureless breccias exposed nearer the centre of the vent (e.g. Fig. 11b). The breccias are interpreted to represent the inner wall of the scoria cone (i.e. wall of the central conduit) and are now largely obscured by late-stage lavas capping the cone. The simplest explanation is that they represent mass wasting of the inner walls of the cone, coupled with repeated explosive evacuation of the vent-fill (cf. Houghton and Schmincke 1989).

Stage 3: final effusive phase

Lava flows near the summit (Fig. 5) overlying the scoria cone deposits (Fig. 2b) likely represent the final phase of volcanic activity at Cabezo María. Given the fact that lavas are apparently cross-cut by late-stage dykes, and considering the mineralogical and geochemical similarities between the flows and dykes (see Table 1, CM4 and CM5a), it is likely that lava flows were fed by small fissure eruptions. The transition from initial hydromagmatic and later Strombolian to effusive activity suggests that the influence of water was minimal in the late stages of eruption (e.g. Houghton and Schmincke 1989; Aranda-Gómez and Luhr 1996; Gernon et al. 2013).

One possible explanation for this eruptive transition is migration of the root zone of the conduit (Fig. 13) downwards below the level of water-saturated sediments (cf. Lorenz 2003). However, there are several alternative explanations, including (1) a lower flux of water into the central 'mixing zone' due to cementation or alteration effects, that decreased the matrix porosity and thus the accessibility of water (Aranda-Gómez and Luhr 1996; Németh et al. 2001); (2) a significant reduction of water entry into the vent by virtue of a rapid increase in magma discharge rate (e.g. Houghton and Schmincke 1989) or (3) exhaustion of water-saturated sediments during earlier eruptions (e.g. Ort and Carrasco-Núñez 2009) and/or a reduced availability of groundwater due to environmental or seasonal effects (e.g. Németh et al. 2001).

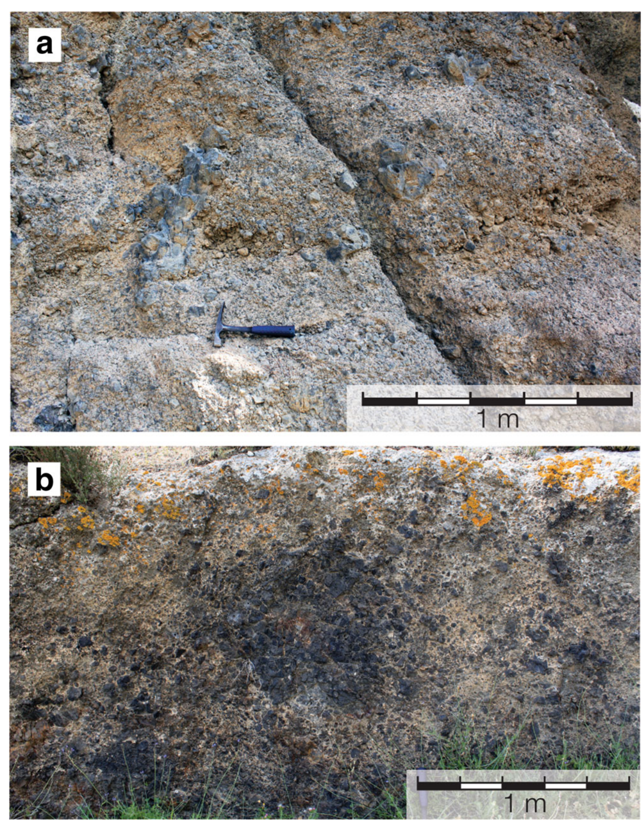

Fig. 11 Field photographs showing detail of bedded scoria deposits shown in Fig. 9a; note the incorporation of spatter bombs. **b** massive lava breccias from near the summit of Cabezo María, SE of the capping lavas (see Fig. 5)

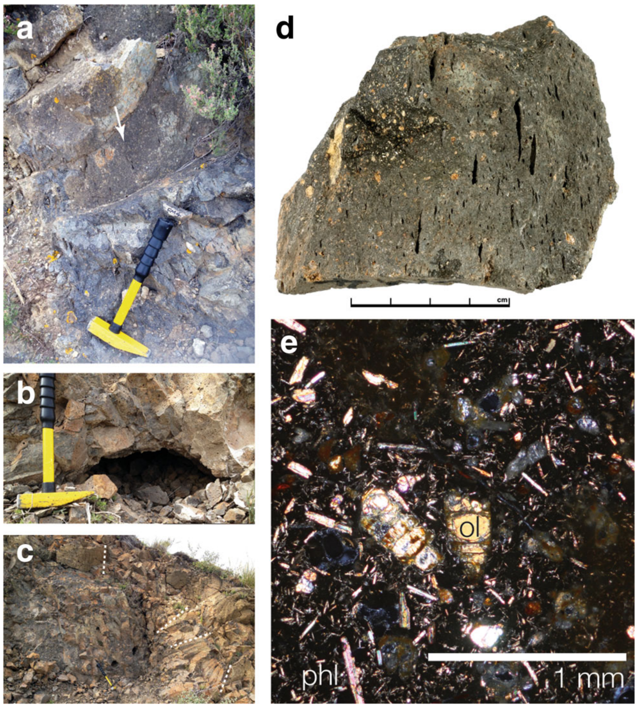

Fig. 12 **a** Field photograph of a dyke exposed at the summit of Cabezo María (see Fig. 5); *arrow* shows stretched vesicle orientation (developed parallel to dyke margins); **b** solidified 'crust' of a lava flow whereby the cavity was formed by lava deflation as a result of lava drainage; **c** well-developed columnar jointing perpendicular the basal surface of a lamproite lava flow (note *dashed lines* show variable orientation); **d** lamproite sample (CM4) from the dyke in (**a**) showing stretched and aligned vesicles and an autolith of lamproite presumably entrained from the underlying lava pile; **e** photomicrograph of the lamproite dyke (**a**) showing olivine crystals (*ol*) and acicular phlogopite crystals (*phl*)

The abundance of crystals in the rocks (Fig. 12d, e) suggest that they were relatively high viscosity, slow-moving lava flows, although the presence of sheared vesicles (Fig. 12d) and inferentially high strain rates may have led to reduced viscosity (e.g. Mader et al. 2013). Nonetheless, the rheological properties of the flows are likely to have encouraged flow-induced auto-brecciation processes, as documented in other lamproite lavas (Williams and McBirney 1979).

Importance of regional tectonics

Lamproite magmatism in the western Mediterranean was associated with major crustal faults that accommodated subduction rollback (Pérez-Valera et al. 2013). Cabezo María volcanism occurred in the context of extensional basin formation and notably a peak in tectonism along the major Palomares Fault Zone (PFZ; Fortuin et al. 1995)—a major NNE-SSW trending sinistral strike-slip fault defining the eastern margin of the Vera Basin (Booth-Rea et al. 2004). Given the radiometric dates and observed relationships between lamproite lavas and sediments, volcanism likely occurred mainly during the Messinian stage. This is supported by the observed occurrence, in other parts of the Vera Basin, of lamproitic lava flows intermixed with slumped Abad Marl Member (lower Messinian), overlying Santiago turbidites (upper part of the Abad Member) (Fortuin et al. 1995), and overlying

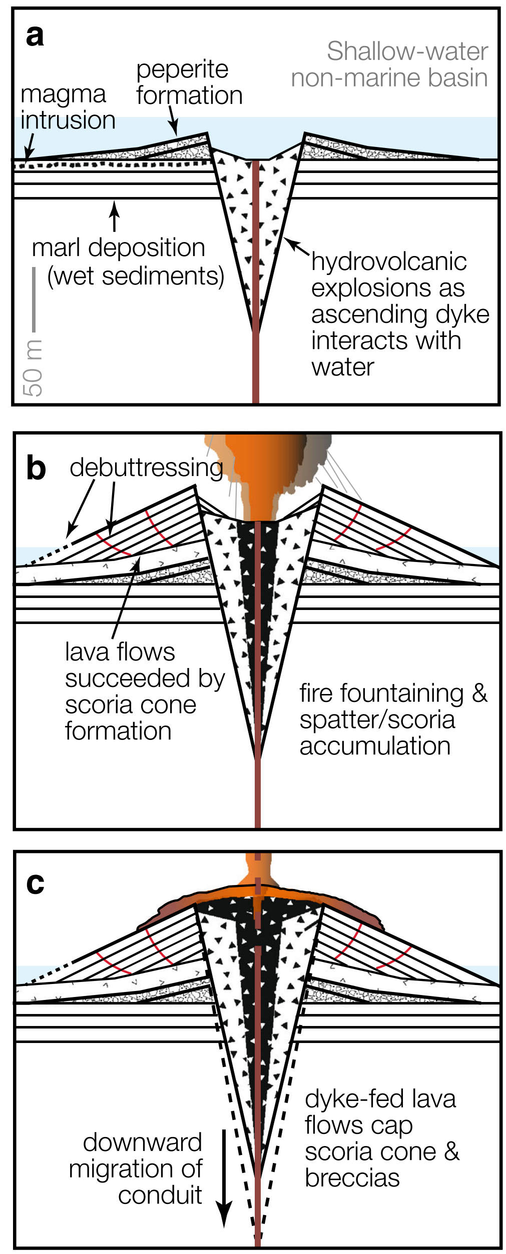

Fig. 13 Schematic cartoon showing the evolution of the Cabezo María edifice, involving **a** explosive magma-water interactions leading to peperite formation, **b** development (above water) of a scoria cone through successive fire fountaining eruptions and **c** downward migration of the conduit (below the level of wet sediments) and a final effusive stage involving dyke-fed eruptions of lava capping the scoria cone

Messinian Cantera carbonates (Völk 1967). At this time, the Vera Basin was open to the Mediterranean Sea, allowing regular seawater incursions (Fortuin et al. 1995)—a factor that might have played a key role in promoting hydromagmatic activity. On the contrary, dyke intrusion, as opposed to magma-sediment interactions and volcanism, was important in the basins further north, for example, Fortuna, Mula and Zeneta (Fig. 1; Seghedi et al. 2007). These ‘inner’ basins were isolated from marine influence and prone to evaporation, possibly explaining the non-explosive emplacement style and apparent lack of features related to magma-water interaction.

Conclusions

Extensive lamproite volcanism in the Betic Cordilleras of SE Spain (i.e. the Murcia-Almeria trend, sensu Mitchell and Bergman 1991) has been attributed to channelling of melts along major crustal faults related to major tectonic processes. The localisation of many lamproite occurrences near the margins of extensional basins indicates a strong regional tectonic control on magmatism. The Cabezo María edifice formed along a fissure network, which initially erupted into a shallow marine-influenced basin, resulting in explosive magma-sediment interactions. Some magmas were intruded along sediment bedding planes causing updoming of beds and mingling at the interface between lavas and sediments. A transition to Strombolian-style eruptions led to progressive growth of a scoria cone and emergence of the system; the growth of the edifice is likely to have accompanied downward migration of a central feeder conduit. The waning phase of volcanism involved fissure eruptions feeding small viscous lava flows that blanketed the underlying inner wall deposits and scoria cone.

The eruption style across the Murcia-Almeria lamproite province is likely to have been governed by the tectonic and environmental context of the host basin(s), which may have been open to marine influence (i.e. outer basin, e.g. Vera) or alternatively may have been restricted and dominated by terrestrial processes (i.e. inner basin, e.g. Fortuna). This may have been particularly important during late Messinian times when basin uplift and isolation, coupled with widespread evaporation, are likely to have favoured non-explosive magma intrusion as opposed to hydromagmatic activity.

Acknowledgments We thank Roberto Sulpizio and Ian Skilling for their very helpful comments and Sonia Calvari for her editorial handling of our manuscript. E.J.R. acknowledges Australian Research Council Laureate Fellowship FL12 0100050.

References

Alonso-Zarza AM et al. (2002) Tertiary. In: The geology of Spain. Geological Society of London

Aranda-Gómez JJ, Luhr JF (1996) Origin of the Joya Honda maar, San Luis Potosí, México. J Volcanol Geotherm Res 74(1–2):1–18

Barton M (1979) A comparative study of some minerals occurring in the potassium-rich alkaline rocks of the Leucite Hills, Wyoming, the Vico volcano, western Italy, and the Toro-Ankole region, Uganda. Neues Jahrb Mineral Abh 137:113–134

Beauchemin D (2008) Inductively coupled plasma mass spectrometry. Anal Chem 80:4455–4486

Bellido Mulas F, Brändle Matesanz J (2011) Neogene Ultrapotassic Volcanism. Gobierno de España, Instituto Geológico y Minero de España, Ch. 13

Booth-Rea G, Azañón J-M, Azor A, Garca-Dueñas V (2004) Influence of strike-slip fault segmentation on drainage evolution and topography. A case study: the Palomares Fault Zone (southeastern Betics, Spain). J Struct Geol 9:1615–1632

Boulter CA (1993) High-level peperitic sills at Rio Tinto, Spain: implications for stratigraphy and mineralization. Trans Inst Min Metall, Sect B 102:30–38

Boulter CA, Wilton VM, Cox DJ, Marshall IS (1999) Magma—wet-sediment interaction: the most widespread yet least recognised alteration system in the Iberian Pyrite Belt. In: Stanley CJ, Balkema AA (eds) Mineral deposits: processes to processing. Brookfield, Vermont, pp 483–486

Boxer G, Lorenz V, Smith CB (1986) The geology and volcanology of the Argyle (AK1) lamproite pipe, Western Australia. In: Procedings of the 4th international kimberlite conference, Perth, Australia. Geological Society of Australia, Sydney, pp 140–152

Brown RJ, Valentine GA (2013) Physical characteristics of kimberlite and basaltic intraplate volcanism and implications of a biased kimberlite record. Geol Soc Am Bull 125(7–8):1224

Brown RJ, Manya S, Buisman I, Fontana G, Field M, MacNiocaill C, Sparks RSJ, Stuart FM (2012) Eruption of kimberlite magmas: physical volcanology, geomorphology and age of the youngest kimberlitic volcanoes known on earth (the Upper Pleistocene/Holocene Igwisi Hills volcanoes, Tanzania). Bull Volcanol 74(7):1621–1643

Busby-Spera C, White JL (1987) Variation in peperite textures associated with differing host-sediment properties. Bull Volcanol 49(6):765–776

Contini S, Venturelli G, Toscani L (1993) Cr-Zr-armalcolite-bearing lamproites of Cancarix, SE Spain. Mineral Mag 57:203–216

Dawson JB (1987) The kimberlite clan: relationship with olivine and leucite lamproites, and inferences for upper-mantle metasomatism. Geol Soc Lond Spec Publ 30:95–101

Duggen S, Hoernle K, Van Den Bogaard P, Garbe-Schönberg D (2005) Post-collisional transition from subduction- to intraplate-type magmatism in the westernmost Mediterranean: evidence for continental-edge delamination of subcontinental lithosphere. J Petrol 46(6):1155–1201

Fortuin AR, Kelling JMD, Roep TB (1995) The enigmatic Messinian-Pliocene section of Cuevas del Almanzora (Vera Basin, SE Spain) revisited—erosional features and strontium isotope ages. Sedi-ment Geol 97(3–4):177–201

Fúster JM, De Pedro F (1953) Estudio petrológico de las rocas volcanicas lamproiticas de Cabezo María (Almeria). Estudios Geologicos 9(20):477–508

Fúster JM, Gastesi P (1965) Estudio petrológico de las rocas lamproíticas de Barqueros (prov. De Murcia). Estud Geol 20:299–314

Gernon TM, Upton BGJ, Hincks TK (2013) Eruptive history of an alkali basaltic diatreme from Elie Ness, Fife, Scotland. Bull Volcanol 75(5):704

Gimeno D (1994) Estudio de las materias primas minerales contenidas en los materiales Miocénicos lacustres de la provincia de Albacete. Al-Basit 34:5–102
Hintz AR, Valentine GA (2012) Complex plumbing of monogenetic scoria cones: new insights from the Lunar Crater Volcanic Field (Nevada, USA). J Volcanol Geotherm Res 239–240:19–32
Hofmann AW (1988) Chemical differentiation of the Earth: the relationship between mantle, continental crust, and oceanic crust. Earth Planet Sci Lett 90(3):297–314
Houghton B, Schmincke H-U (1989) Rothenberg scoria cone, East Eifel: a complex Strombolian and phreatomagmatic volcano. Bull Volcanol 52(1)
Imai N, Terashima S, Itoh S, Ando A (1995) 1994 compilation of analytical data for minor and trace elements in seventeen GSJ geochemical reference samples, "Igneous rock series". Geostand Newslett 19:135–213
Kiyosugi K, Connor CB, Wetmore PH, Ferwerda BP, Germa AM, Connor LJ, Hintz AR (2012) Relationship between dike and volcanic conduit distribution in a highly eroded monogenetic volcanic field: San Rafael, Utah, USA. Geology 40(8):695–698
Kokelaar BP (1982) Fluidization of wet sediments during the emplacement and cooling of various igneous bodies. J Geol Soc Lond 139(1):21–33
Lorenz V (2003) Maar-diatreme volcanoes, their formation, and their setting in hard-rock or soft-rock environments. Geolines 15:72–83
Mader HM, Llewellin EW, Mueller SP (2013) The rheology of two-phase magmas: a review and analysis. J Volcanol Geotherm Res 257:135–158
Middlemost EAK (1975) The basalt clan. Earth-Sci Rev 11:337–364
Mitchell RH, Bergman SC (1991) Petrology of lamproites. Springer
Montenat C, Thaler I, Couvering JV (1975) La faune rougeurs de Librilla. Correlation avec les formations marines du Miocene terminal et les datations radiometriques du volcanisme de Barqueros (Province de Murcia, Espagne meridionale). C R Acad Sci Paris 281:519–522
Murton B, Taylor R, Thirlwall M (2002) Plume-ridge interaction: a geochemical perspective from the Reykjanes Ridge. J Petrol 43(11):1987–2012
Németh K, Martin U, Harangi S (2001) Miocene phreatomagmatic volcanism at Tihany (Pannonian Basin, Hungary). J Volcanol Geotherm Res 111:111–135
Nixon PH, Thirlwall MF, Buckley F, Davies CJ (1984) Spanish and western Australian lamproites: aspects of whole rock geochemistry. Vol. Kimerlites and related rocks, Elsevier, pp 285–296
Nobel FA, Andriessen PAM, Hebeda EH, Priem HNA (1981) Isotopic dating of the post-Alpine Neogene volcanism in the Betic Cordilleras, southern Spain. Geol Mijnb 60(2):209–214
Ort MH, Carrasco-Núñez G (2009) Lateral vent migration during phreatomagmatic and magmatic eruptions at Tecuitlapa Maar, east-central Mexico. J Volcanol Geotherm Res 181(1–2):67–77
Pearson DG, Davies GR, Nixon PH, Greenwood PB, Mattey DP (1991) Oxygen isotope evidence for the origin of pyroxenites in the Beni Bousera peridotite massif, North Morocco: derivation from subducted oceanic lithosphere. Earth Planet Sci Lett 102(3–4):289–301
Pérez-Valera LA, Rosenbaum G, Sánchez-Gómez M, Azor A, Fernández-Soler JM, Pérez-Valera F, Vasconcelos PM (2013) Age distribution of lamproites along the Socovos Fault (southern Spain) and lithospheric scale tearing. Lithos 180–181:252–263
Playà E, Gimeno D (2006) Evaporite deposition and coeval volcanism in the Fortuna Basin (Neogene, Murcia, Spain). Sediment Geol 188–189:205–218
Seghedi I, Szakács A, Pacheco AH, Matesanz J-LB (2007) Miocene lamproite volcanoes in south-eastern Spain—an association of phreatomagmatic and magmatic products. J Volcanol Geotherm Res 159(1–3):210–224
Skilling IP, White JDL, McPhie J (2002) Peperite: a review of magma–sediment mingling. J Volcanol Geotherm Res 114(1–2):1–17
Sparks RSJ, Baker L, Brown R, Field M, Schumacher J, Stripp G, Walters A (2006) Dynamical constraints on kimberlite volcanism. J Volcanol Geotherm Res 155:18–48
Stachel T, Lorenz V, Smith CB, Jaques AL (1991) Evolution of four individual lamproite pipes, Ellendale volcanic field (Western Australia). In: Meyer H, Leonardos O (eds) Proceedings of the 5th international kimberlite conference. Araxa, Brazil, pp 177–194
Sun S-S (1982) Chemical composition and origin of the earth's primitive mantle. Geochim Cosmochim Acta 46(2):179–192
Turner S, Hawkesworth C (1995) The nature of the sub-continental mantle: constraints from the major-element composition of continental flood basalts. Chem Geol 120(3–4):295–314
Turner SP, Platt JP, George RMM, Kelley SP, Pearson DG, Nowell GM (1999) Magmatism associated with orogenic collapse of the Betic–Alboran domain, SE Spain. J Petrol 40(6):1011–1036
Venturelli G, Capedri S, Di Battistini G, Crawford A, Kogarko LN, Celestini S (1984) The ultrapotassic rocks from southeastern Spain. Lithos 17:37–54
Völk HR (1967) Zur Geologie und Stratigraphie des Neogenbeckens von Vera. Ph.D. thesis, Univ. of Amsterdam
Williams H, McBirney AR (1979) Volcanology. Freeman, San Francisco